

# A time-reversible integrator for the time-dependent Schrödinger equation on an adaptive grid

Seonghoon Choi and Jiří Vaníček<sup>a)</sup>

*Laboratory of Theoretical Physical Chemistry, Institut des Sciences et Ingénierie Chimiques, Ecole Polytechnique Fédérale de Lausanne (EPFL), CH-1015, Lausanne, Switzerland*

(Dated: 17 September 2019)

One of the most accurate methods for solving the time-dependent Schrödinger equation uses a combination of the dynamic Fourier method with the split-operator algorithm on a tensor-product grid. To reduce the number of required grid points, we let the grid move together with the wavepacket, but find that the naïve algorithm based on an alternate evolution of the wavefunction and grid destroys the time reversibility of the exact evolution. Yet, we show that the time reversibility is recovered if the wavefunction and grid are evolved simultaneously during each kinetic or potential step; this is achieved by using the Ehrenfest theorem together with the splitting method. The proposed algorithm is conditionally stable, symmetric, time-reversible, and conserves the norm of the wavefunction. The preservation of these geometric properties is shown analytically and demonstrated numerically on a three-dimensional harmonic model and collinear model of He–H<sub>2</sub> scattering. We also show that the proposed algorithm can be symmetrically composed to obtain time-reversible integrators of an arbitrary even order. We observed 10000-fold speedup by using the tenth- instead of the second-order method to obtain a solution with a time discretization error below 10<sup>-10</sup>. Moreover, using the adaptive grid instead of the fixed grid resulted in a 64-fold reduction in the required number of grid points in the harmonic system and made it possible to simulate the He–H<sub>2</sub> scattering for six times longer, while maintaining reasonable accuracy.

## I. INTRODUCTION

Understanding many dynamical phenomena in chemical physics requires the solution of the time-dependent Schrödinger equation.<sup>1–7</sup> This equation can be often solved both accurately and efficiently by employing a combination of the dynamic Fourier method with a high-order split-operator algorithm<sup>8–12</sup> on a tensor-product grid.<sup>8,9,13</sup> However, for simulations that access only a small portion of the tensor-product Hilbert space, more suitable methods exist. These methods focus the available computational resources on the important portions of the full Hilbert space.

The multiconfigurational time-dependent Hartree (MCTDH) method<sup>14–16</sup> and its multilayer extension<sup>17</sup> reduce the required number of basis functions by employing an optimized time-dependent basis set. Similarly, sparse-grid methods<sup>10,18–20</sup> reduce the number of required grid points. They achieve this, e.g., by employing the Smolyak quadrature.<sup>21</sup> Making the grid adaptive<sup>22</sup> is another common approach to reduce the required number of grid points. For example, the adaptive moving grid has been used to improve the quantum trajectory method<sup>23,24</sup> near wavefunction nodes,<sup>25–27</sup> to treat the interaction of molecules with intense time-dependent electromagnetic fields,<sup>28</sup> and to reduce the size<sup>29–31</sup> of grids employed in discrete variable representation (DVR).<sup>32</sup>

To reduce the number of grid points and memory required for quantum simulations of systems that occupy

only a small part of the accessible phase-space at any given time, in this paper, we use an adaptive tensor-product grid that moves according to the wavepacket's position and momentum expectation values. The most naïve approach is to evolve the grid only after each time step of the wavefunction propagation. However, this naïve grid adaptation breaks the symmetry and, therefore, also the time reversibility of the time propagation scheme.

We find that the time reversibility is recovered when the grid is evolved simultaneously with the wavepacket. The resulting algorithm is not only symmetric and time-reversible, but also norm-preserving and conditionally stable (i.e., stable for small enough time steps). In addition, because of its symmetry, this algorithm can be composed by various symmetric composition schemes to obtain higher-order integrators.<sup>11,12,33–36</sup>

The remainder of this paper is organized as follows: In Sec. II, we give a brief overview of the split-operator algorithm and dynamic Fourier method, including their discretized implementation on a tensor-product grid. Then, we demonstrate the breakdown of the time reversibility by the naïve grid adaptation, and the recovery of the time reversibility by employing a combination of the Ehrenfest theorem<sup>37</sup> and splitting method.<sup>10,11</sup> In Sec. III, we numerically confirm the geometric and convergence properties of the proposed algorithm using a three-dimensional harmonic model of electronic excitation and a two-dimensional modified Secret–Johnson<sup>38,39</sup> model of He–H<sub>2</sub> scattering. Section IV concludes the paper.

<sup>a)</sup>Electronic mail: jiri.vanicek@epfl.ch

## II. THEORY

The time-dependent Schrödinger equation,

$$\frac{d|\psi_t\rangle}{dt} = -\frac{i}{\hbar}\hat{H}|\psi_t\rangle, \quad (1)$$

where  $\hat{H}$  is a time-independent Hamiltonian and  $|\psi_t\rangle$  is the quantum state at time  $t$ , has the solution  $|\psi_t\rangle = \hat{U}(t)|\psi_0\rangle$  with the exact evolution operator  $\hat{U}(t) := e^{-it\hat{H}/\hbar}$ . In general, this exact solution must be approximated by one of many possible time propagation schemes. Here, we will only discuss the split-operator algorithms<sup>8–10</sup> in detail because the splitting method<sup>10,11</sup> is crucial for the time-reversible grid adaptation that we derive in Sec. II G.

### A. Split-operator algorithm and dynamic Fourier method

The splitting method requires the Hamiltonian to be separable into a sum of kinetic and potential energy operators:

$$\hat{H} = T(\hat{\vec{p}}) + V(\hat{\vec{q}}), \quad (2)$$

where  $\vec{p}$  and  $\vec{q}$  are  $D$ -dimensional momentum and position, respectively. For orthogonal coordinates, the kinetic energy  $T(\vec{p})$  has a simple form

$$T(\vec{p}) = \frac{1}{2}\vec{p}^T \cdot m^{-1} \cdot \vec{p}, \quad (3)$$

where  $m$  is a real symmetric (and often diagonal)  $D \times D$  mass matrix. For Hamiltonians of form (2), all split-operator algorithms can be expressed as a composition<sup>11</sup> of kinetic  $[\hat{U}_{\hat{T}}(t)]$  and potential  $[\hat{U}_{\hat{V}}(t)]$  evolution operators, where  $\hat{U}_{\hat{A}}(t) := e^{-it\hat{A}/\hbar}$  is the exact evolution operator for a Hamiltonian  $\hat{H} = \hat{A}$ . The simplest first-order split-operator algorithm<sup>40</sup> has the approximate evolution operator

$$\hat{U}_{\text{TV}}(\Delta t) := \hat{U}_{\hat{T}}(\Delta t)\hat{U}_{\hat{V}}(\Delta t). \quad (4)$$

This ‘‘TV’’ algorithm can be composed with its adjoint,  $\hat{U}_{\text{VT}}(\Delta t) := \hat{U}_{\text{TV}}(-\Delta t)^{-1}$ , to obtain the second-order TVT algorithm,<sup>41</sup>

$$\begin{aligned} \hat{U}_{\text{TVT}}(\Delta t) &:= \hat{U}_{\text{TV}}(\Delta t/2)\hat{U}_{\text{VT}}(\Delta t/2) \\ &= \hat{U}_{\hat{T}}(\Delta t/2)\hat{U}_{\hat{V}}(\Delta t)\hat{U}_{\hat{T}}(\Delta t/2), \end{aligned} \quad (5)$$

which is symmetric, i.e., satisfies  $\hat{U}_{\text{TVT}}(\Delta t) = \hat{U}_{\text{TVT}}(-\Delta t)^{-1}$ . Because it is symmetric, the TVT algorithm can be recursively composed by symmetric schemes<sup>10,11,33–36</sup> to obtain symmetric algorithms

$$\hat{U}_{\text{comp}}(\Delta t) := \hat{U}_{\text{TVT}}(\gamma_{N_{\text{comp}}}\Delta t) \cdots \hat{U}_{\text{TVT}}(\gamma_1\Delta t) \quad (6)$$

of arbitrary even orders of accuracy in the time step, where  $\gamma_k$  is the  $k$ th composition coefficient (with

$\sum_{k=1}^{N_{\text{comp}}} \gamma_k = 1$ ,  $\gamma_{N_{\text{comp}}+1-k} = \gamma_k$ ) and  $N_{\text{comp}}$  is the number of composition steps. [Exchanging  $V$  and  $T$  in algorithms (4)–(6) results in another set of split-operator algorithms.] The higher-order algorithms, despite their higher computational cost per time step, are often more efficient if high accuracy is desired. Moreover, all symmetric split-operator algorithms are examples of geometric integrators because they preserve many important geometric properties of the exact solution of Eq. (1), namely linearity, unitarity, symplecticity, stability, symmetry, and time reversibility.<sup>10,11,42</sup> For additional details about the properties and numerical implementation of the higher-order split-operator algorithms, we refer the reader to Ref. 12.

The action of compositions of  $\hat{U}_{\hat{T}}(\Delta t)$  and  $\hat{U}_{\hat{V}}(\Delta t)$  on  $|\psi\rangle$  is simply evaluated using the dynamic Fourier method<sup>8,9,13</sup> in which the action of a function  $g(\hat{\vec{x}})$  of an operator  $\hat{\vec{x}}$  on the wavepacket  $|\psi\rangle$  is evaluated as  $g(\vec{x})\psi(\vec{x})$  in the  $\vec{x}$ -representation, where  $\vec{x}$  is either the position  $\vec{q}$  or momentum  $\vec{p}$ . The wavefunction is transformed, if required, to the  $\vec{x}$ -representation by either the Fourier or inverse Fourier transformation:

$$\tilde{\psi}(\vec{p}) = (2\pi\hbar)^{-D/2} \int \psi(\vec{q}) e^{-i\vec{p}\cdot\vec{q}/\hbar} d^D q, \quad (7)$$

$$\psi(\vec{q}) = (2\pi\hbar)^{-D/2} \int \tilde{\psi}(\vec{p}) e^{i\vec{p}\cdot\vec{q}/\hbar} d^D p, \quad (8)$$

where  $\vec{p} \cdot \vec{q} := \sum_{l=1}^D p_l q_l$ .

### B. Dynamic Fourier method on a grid

The dynamic Fourier method on a grid follows the same approach as in Sec. II A except that  $g(\vec{x})\psi(\vec{x})$  and the integral transforms (7) and (8) are now discretized on a grid, consisting of points  $\vec{x}^I$  for all  $I \in \mathcal{I}$ . Here, the multi-index  $I = (i_1, \dots, i_D)$  is an ordered  $D$ -tuple of integers from the set  $\mathcal{I}$  of all admissible multi-indices, where

$$\begin{aligned} \mathcal{I} &:= \{(i_1, \dots, i_D) : i_l \in \{0, \dots, N_l - 1\} \\ &\text{for all } l \in \{1, \dots, D\}\}, \end{aligned} \quad (9)$$

and  $N_l$  is the number of grid points in the  $l$ th dimension. When iterating over all admissible multi-indices, we will simply write  $I \in \mathcal{I}$ . The  $D$  coordinates of the grid point  $\vec{x}^I$  are given by

$$x_l^I := x_{\text{ctr},l} + (i_l - N_l/2)\Delta x_l \quad \text{for } l \in \{1, \dots, D\}, \quad (10)$$

where  $\vec{x}_{\text{ctr}}$  is the  $\vec{x}$ -grid center and  $\Delta\vec{x}$  are the  $\vec{x}$ -spacings of the grid. Note that  $\Delta q_l \Delta p_l = 2\pi\hbar/N_l$ .

Application of the operator  $g(\hat{\vec{x}})$  to  $\psi$  in  $\vec{x}$ -representation is given by

$$g(\vec{x})\psi(\vec{x}) \stackrel{\text{grid}}{=} g(\vec{x}^I)\psi(\vec{x}^I), \quad (11)$$

where  $\stackrel{\text{grid}}{=}$  denotes “is represented on a grid as.” The integral transforms (7) and (8) are discretized on a grid as

$$\tilde{\psi}(\vec{p}^K) = C_q \sum_{J \in \mathcal{I}} \psi(\vec{q}^J) e^{-i\vec{p}^K \cdot \vec{q}^J / \hbar}, \quad K \in \mathcal{I}, \quad (12)$$

$$\psi(\vec{q}^J) = C_p \sum_{K \in \mathcal{I}} \tilde{\psi}(\vec{p}^K) e^{i\vec{p}^K \cdot \vec{q}^J / \hbar}, \quad J \in \mathcal{I}, \quad (13)$$

with prefactors  $C_x := \prod_{l=1}^D (\Delta x_l / \sqrt{2\pi\hbar})$ . To express Eqs. (12) and (13) in terms of the standard discrete Fourier transform (DFT), we scale the wavefunctions as  $\tilde{\psi}^K := \tilde{\psi}(\vec{p}^K) / \sqrt{C_q}$ ,  $\psi^J := \psi(\vec{q}^J) / \sqrt{C_p}$  and use Eq. (10). As a result, we obtain

$$\tilde{\psi}^K = \frac{1}{\sqrt{N}} \sum_{J \in \mathcal{I}} e^{-2\pi i \langle K, J \rangle} e^{-it_{KJ} / \hbar} \psi^J, \quad K \in \mathcal{I}, \quad (14)$$

$$\psi^J = \frac{1}{\sqrt{N}} \sum_{K \in \mathcal{I}} e^{2\pi i \langle J, K \rangle} e^{it_{KJ} / \hbar} \tilde{\psi}^K, \quad J \in \mathcal{I}, \quad (15)$$

where  $N := \prod_{l=1}^D N_l$  denotes the total number of grid points,

$$t_{KJ} = \sum_{l=1}^D [(p_{\text{ctr},l} - \Delta p_l N_l / 2)(q_{\text{ctr},l} - \Delta q_l N_l / 2) + p_{\text{ctr},l} j_l \Delta q_l + q_{\text{ctr},l} k_l \Delta p_l - \pi \hbar (j_l + k_l)], \quad (16)$$

and the multi-index inner product  $\langle K, J \rangle := \sum_{l=1}^D k_l j_l / N_l$ . The scaled wavefunction  $\tilde{\psi}^K$  can be viewed as a standard DFT of  $e^{-it_{KJ} / \hbar} \psi^J$  and  $\psi^J$  as a standard inverse DFT of  $e^{it_{KJ} / \hbar} \tilde{\psi}^K$ . In practice, the DFT is implemented using the celebrated fast Fourier transform algorithm.<sup>43</sup>

### C. Shifting the grid

In Sec. II B, we assumed the grid centers to be fixed, but this assumption will now be dropped to allow for grid shifting. Moreover, all quantities defined in Sec. II B will be re-expressed in a more compact matrix form. Equations (14) and (15) thus become

$$\tilde{\psi}(\vec{p}_{\text{ctr}}) = \mathbf{f}(\vec{q}_{\text{ctr}}, \vec{p}_{\text{ctr}}) \psi(\vec{q}_{\text{ctr}}), \quad (17)$$

$$\psi(\vec{q}_{\text{ctr}}) = \tilde{\mathbf{f}}(\vec{q}_{\text{ctr}}, \vec{p}_{\text{ctr}}) \tilde{\psi}(\vec{p}_{\text{ctr}}), \quad (18)$$

where the “vectors”  $\psi(\vec{q}_{\text{ctr}})$  and  $\tilde{\psi}(\vec{p}_{\text{ctr}})$  are rank- $D$  tensors with  $N$  components  $\psi^J(\vec{q}_{\text{ctr}})$  and  $\tilde{\psi}^K(\vec{p}_{\text{ctr}})$ , respectively, and the “matrices” representing the Fourier transforms are

$$[\mathbf{f}(\vec{q}_{\text{ctr}}, \vec{p}_{\text{ctr}})]_{KJ} := \frac{1}{\sqrt{N}} e^{-2\pi i \langle K, J \rangle} e^{-it_{KJ}(\vec{q}_{\text{ctr}}, \vec{p}_{\text{ctr}}) / \hbar}, \quad (19)$$

$$\tilde{\mathbf{f}}(\vec{q}_{\text{ctr}}, \vec{p}_{\text{ctr}}) = \mathbf{f}(\vec{q}_{\text{ctr}}, \vec{p}_{\text{ctr}})^{-1} = \mathbf{f}(\vec{q}_{\text{ctr}}, \vec{p}_{\text{ctr}})^\dagger; \quad (20)$$

in Eqs. (17) and (18), a compact notation for the “matrix-vector” multiplication, defined by  $(\mathbf{a}\psi)_K := \sum_{J \in \mathcal{I}} a_{KJ} \psi^J$ ,  $K \in \mathcal{I}$ , is employed, and  $\tilde{\cdot}$  above a matrix denotes that it is applied to a wavefunction in the  $\vec{p}$ -representation.

Equation (18) expresses that the momentum wavefunction  $\tilde{\psi}(\vec{p}_{\text{ctr}})$  represented on the  $\vec{p}$ -grid centered at  $\vec{p}_{\text{ctr}}$  is transformed to the position wavefunction  $\psi(\vec{q}_{\text{ctr}})$  represented on the  $\vec{q}$ -grid centered at  $\vec{q}_{\text{ctr}}$  by applying  $\tilde{\mathbf{f}}(\vec{q}_{\text{ctr}}, \vec{p}_{\text{ctr}})$ . Similarly,  $\psi(\vec{q}_{\text{ctr}})$  is transformed to  $\tilde{\psi}(\vec{p}_{\text{ctr}})$  by applying  $\mathbf{f}(\vec{q}_{\text{ctr}}, \vec{p}_{\text{ctr}})$  according to Eq. (17).

### D. Split-operator algorithm on a grid

Kinetic and potential evolution operators  $\hat{U}_{\hat{T}}(\Delta t)$  and  $\hat{U}_{\hat{V}}(\Delta t)$ , which are composed to obtain any split-operator algorithm (see Sec. II A), are discretized on a grid as diagonal finite-dimensional tensors

$$[\mathbf{U}_V(\Delta t, \vec{q}_{\text{ctr}})]_{JJ'} = \delta_{JJ'} e^{-i\Delta t V(\vec{q}^J(\vec{q}_{\text{ctr}})) / \hbar}, \quad (21)$$

$$[\tilde{\mathbf{U}}_T(\Delta t, \vec{p}_{\text{ctr}})]_{KK'} = \delta_{KK'} e^{-i\Delta t T(\vec{p}^K(\vec{p}_{\text{ctr}})) / \hbar}. \quad (22)$$

Therefore, the time-evolved wavefunctions are

$$\langle \vec{q} | \hat{U}_{\hat{V}}(\Delta t) | \psi \rangle \stackrel{\text{grid}}{=} \sqrt{C_p} \mathbf{U}_V(\Delta t, \vec{q}_{\text{ctr}}) \psi(\vec{q}_{\text{ctr}}), \quad (23)$$

$$\langle \vec{p} | \hat{U}_{\hat{T}}(\Delta t) | \psi \rangle \stackrel{\text{grid}}{=} \sqrt{C_q} \tilde{\mathbf{U}}_T(\Delta t, \vec{p}_{\text{ctr}}) \tilde{\psi}(\vec{p}_{\text{ctr}}); \quad (24)$$

note that the scaled wavefunctions,  $\psi^J$  and  $\tilde{\psi}^K$ , must be scaled back to  $\psi(\vec{q}^J)$  and  $\tilde{\psi}(\vec{p}^K)$  at the end of the propagation with factors  $\sqrt{C_p}$  and  $\sqrt{C_q}$ , respectively (see Sec II B).

### E. Loss of linearity by the grid adaptation

To be specific, we now assume that the initial wavefunction is provided in the  $\vec{q}$ -representation and that the solution at time  $t$  is desired also in the  $\vec{q}$ -representation. Let the adaptive  $\vec{x}$ -grid be centered at the wavefunction’s  $\vec{x}$ -expectation value. The resulting equations of motion for the wavefunction and grid centers,  $\vec{x}_t := \vec{x}_{\text{ctr}}(t)$ , are

$$\dot{\psi}_t(\vec{q}_t) = -\frac{i}{\hbar} \mathbf{H}(\vec{q}_t, \vec{p}_t) \psi_t(\vec{q}_t), \quad (25)$$

$$\dot{\vec{q}}_t = \langle \vec{\mathbf{q}}(\vec{q}_t) \rangle_{\psi_t(\vec{q}_t)}, \quad (26)$$

$$\dot{\vec{p}}_t = \langle \vec{\mathbf{p}}(\vec{p}_t) \rangle_{\tilde{\psi}_t(\vec{p}_t)}, \quad (27)$$

where  $\tilde{\psi}_t(\vec{p}_t) = \mathbf{f}(\vec{q}_t, \vec{p}_t) \psi_t(\vec{q}_t)$ ,  $\mathbf{H}(\vec{q}_t, \vec{p}_t)$  is the Hamiltonian in the  $\vec{q}$ -representation, containing appropriate Fourier transforms, and represented on the grid centered at  $\vec{x}_t$ ,  $[\vec{\mathbf{x}}(\vec{x}_t)]_{II'} := \delta_{II'} \vec{x}^I(\vec{x}_t)$ , and  $\langle \mathbf{O}(\vec{x}_t) \rangle_{\psi_t(\vec{x}_t)} := \langle \psi_t(\vec{x}_t) | \mathbf{O}(\vec{x}_t) \psi_t(\vec{x}_t) \rangle$ ; the inner product between  $\psi$  and  $\phi$  is defined as

$$\langle \psi(\vec{x}_t) | \phi(\vec{x}_t) \rangle := \left( \prod_{l=1}^D \Delta x_l \right) \sum_{I \in \mathcal{I}} \psi(\vec{x}^I(\vec{x}_t))^* \phi(\vec{x}^I(\vec{x}_t)). \quad (28)$$

The grid adaptation leads to the loss of some geometric properties even if Eqs. (25)–(27) are solved exactly. In Eq. (25), the Hamiltonian is nonlinear due to its dependence on  $\psi_t$  (via  $\vec{q}_t$  and  $\vec{p}_t$ ); the corresponding evolution operator is, therefore, also nonlinear, and does not preserve the inner product.<sup>44</sup> As a consequence, the symplectic two-form<sup>10</sup>  $\omega(\psi, \phi) := -2\hbar\text{Im}\langle\psi|\phi\rangle$  is not preserved, either. In contrast, the exact solution of Eqs. (25)–(27) does preserve the norm and is both symmetric and time-reversible.

### F. Loss of time reversibility by the naïve adaptive grid

Due to their mutual coupling, Eqs. (25)–(27) cannot be, in general, solved analytically. The naïve adaptive grid approximation decouples the equations for the wavefunction and grid evolutions by first solving Eq. (25) for  $\psi_t$  with fixed  $\vec{q}_t$  and  $\vec{p}_t$  during the time  $0 \leq t \leq \Delta t$ , obtaining  $\psi_{\Delta t}(\vec{q}_0) = \mathbf{U}(\Delta t; \vec{q}_0, \vec{p}_0)\psi_0(\vec{q}_0)$ , where

$$\mathbf{U}(\Delta t; \vec{q}_0, \vec{p}_0) := e^{-i\Delta t\mathbf{H}(\vec{q}_0, \vec{p}_0)/\hbar}. \quad (29)$$

The grid centers are then updated using the propagated wavefunction  $\psi_{\Delta t}(\vec{q}_0)$ :

$$\vec{q}_{\Delta t} = \langle\vec{\mathbf{q}}(\vec{q}_0)\rangle_{\psi_{\Delta t}(\vec{q}_0)}, \quad (30)$$

$$\vec{p}_{\Delta t} = \langle\vec{\mathbf{p}}(\vec{p}_0)\rangle_{\tilde{\psi}_{\Delta t}(\vec{p}_0)}. \quad (31)$$

Finally, the wavefunction  $\psi_{\Delta t}(\vec{q}_0)$  is represented on the updated grid:

$$\tilde{\psi}_{\Delta t}(\vec{p}_{\Delta t}) = \mathbf{f}(\vec{q}_0, \vec{p}_{\Delta t})\psi_{\Delta t}(\vec{q}_0), \quad (32)$$

$$\psi_{\Delta t}(\vec{q}_{\Delta t}) = \tilde{\mathbf{f}}(\vec{q}_{\Delta t}, \vec{p}_{\Delta t})\tilde{\psi}_{\Delta t}(\vec{p}_{\Delta t}). \quad (33)$$

The overall evolution operator for the naïve adaptive grid is, therefore,

$$\begin{aligned} \mathbf{U}_{\text{naïve}}(\Delta t; \psi_0, \vec{q}_0, \vec{p}_0) \\ := \tilde{\mathbf{f}}(\vec{q}_{\Delta t}, \vec{p}_{\Delta t})\mathbf{f}(\vec{q}_0, \vec{p}_{\Delta t})\mathbf{U}(\Delta t; \vec{q}_0, \vec{p}_0), \end{aligned} \quad (34)$$

where the dependence of  $\mathbf{U}_{\text{naïve}}$  on  $\psi_0$  comes from the dependence of  $\vec{q}_{\Delta t}$  and  $\vec{p}_{\Delta t}$  on  $\psi_0$ .

The time propagation on the naïve adaptive grid preserves the norm  $\|\psi_t(\vec{q}_t)\| := \langle\psi_t(\vec{q}_t)|\psi_t(\vec{q}_t)\rangle^{1/2}$  because  $\mathbf{U}_{\text{naïve}}$  is a composition of three norm-preserving operators: That  $\mathbf{f}$  and  $\tilde{\mathbf{f}}$  preserve the norm follows from Eq. (20), and  $\mathbf{U}(\Delta t, \vec{q}_0, \vec{p}_0)$  preserves the norm because  $\mathbf{U}^\dagger = \mathbf{U}^{-1}$  [see Eq. (29)].

A symmetric operator is time-reversible [i.e., satisfies  $\mathbf{U}(-\Delta t)\mathbf{U}(\Delta t) = 1$ ] and vice versa. Both of these properties are lost in the naïve adaptive grid approach because

$$\begin{aligned} \mathbf{U}_{\text{naïve}}(-\Delta t; \psi_{\Delta t}, \vec{q}_{\Delta t}, \vec{p}_{\Delta t})\mathbf{U}_{\text{naïve}}(\Delta t; \psi_0, \vec{q}_0, \vec{p}_0) \\ = \tilde{\mathbf{f}}(\vec{q}_0', \vec{p}_0')\mathbf{f}(\vec{q}_{\Delta t}, \vec{p}_0')\mathbf{U}(-\Delta t; \vec{q}_{\Delta t}, \vec{p}_{\Delta t}) \\ \times \tilde{\mathbf{f}}(\vec{q}_{\Delta t}, \vec{p}_{\Delta t})\mathbf{f}(\vec{q}_0, \vec{p}_{\Delta t})\mathbf{U}(\Delta t; \vec{q}_0, \vec{p}_0) \neq 1, \end{aligned} \quad (35)$$

where

$$\vec{q}_0' = \langle\vec{\mathbf{q}}(\vec{q}_{\Delta t})\rangle_{\psi_0(\vec{q}_{\Delta t})} \neq \vec{q}_0, \quad (36)$$

$$\vec{p}_0' = \langle\vec{\mathbf{p}}(\vec{p}_{\Delta t})\rangle_{\tilde{\psi}_0(\vec{p}_{\Delta t})} \neq \vec{p}_0, \quad (37)$$

$$\psi_0(\vec{q}_{\Delta t}) = \mathbf{U}(-\Delta t; \vec{q}_{\Delta t}, \vec{p}_{\Delta t})\psi_{\Delta t}(\vec{q}_{\Delta t}), \quad (38)$$

$$\tilde{\psi}_0(\vec{p}_{\Delta t}) = \mathbf{f}(\vec{q}_{\Delta t}, \vec{p}_{\Delta t})\psi_0(\vec{q}_{\Delta t}). \quad (39)$$

Note that inequality (35) would still hold even in the unlikely situation that, by chance,  $\vec{q}_0' = \vec{q}_0$  and  $\vec{p}_0' = \vec{p}_0$ . As we shall see below, to preserve the symmetry and time reversibility, the grid must be evolved simultaneously with the wavefunction.

### G. Recovery of time reversibility by a combination of the splitting method and Ehrenfest theorem

The Ehrenfest theorem<sup>37</sup> states that the time derivatives of the position and momentum expectation values satisfy

$$\dot{\vec{q}}_t = \langle\partial\mathbf{H}/\partial\vec{p}(\vec{q}_t, \vec{p}_t)\rangle_{\psi_t(\vec{q}_t)}, \quad (40)$$

$$\dot{\vec{p}}_t = -\langle\partial\mathbf{H}/\partial\vec{q}(\vec{q}_t, \vec{p}_t)\rangle_{\psi_t(\vec{q}_t)}. \quad (41)$$

The system of differential and algebraic Eqs. (25), (26), (27) for  $\psi_t, \vec{q}_t, \vec{p}_t$  is equivalent to and, hence, can be replaced with the system of differential Eqs. (25), (40), (41). These equations can be solved analytically if  $\hat{H} = V(\hat{q})$  or  $\hat{H} = T(\hat{p})$ . This is the essence of the splitting method<sup>10,11</sup> (see Sec. II A).

#### 1. Potential propagation: $\hat{H} = V(\hat{q})$

When  $\hat{H} = V(\hat{q})$ , Eqs. (25), (40), (41) become

$$\dot{\psi}_t(\vec{q}_t) = -\frac{i}{\hbar}\mathbf{V}(\vec{q}_t)\psi_t(\vec{q}_t), \quad (42)$$

$$\dot{\vec{q}}_t = 0, \quad (43)$$

$$\dot{\vec{p}}_t = -\langle\partial\mathbf{V}/\partial\vec{q}(\vec{q}_t)\rangle_{\psi_t(\vec{q}_t)}, \quad (44)$$

where  $[\mathbf{V}(\vec{q}_t)]_{JJ'} = \delta_{JJ'}V(\vec{q}^J(\vec{q}_t))$ . These equations have an exact analytical solution for arbitrarily long time  $t$ , namely:

$$\psi_t(\vec{q}_t) = \mathbf{U}_V(t, \vec{q}_0)\psi_0(\vec{q}_0), \quad (45)$$

$$\vec{q}_t = \vec{q}_0, \quad (46)$$

$$\vec{p}_t = \vec{p}_0 - t\langle\partial\mathbf{V}/\partial\vec{q}(\vec{q}_0)\rangle_{\psi_0(\vec{q}_0)}. \quad (47)$$

## 2. Kinetic propagation: $\hat{H} = T(\hat{\vec{p}})$

Similarly, when  $\hat{H} = T(\hat{\vec{p}})$ , Eqs. (25), (40), (41) become

$$\dot{\tilde{\psi}}_t(\vec{p}_t) = -\frac{i}{\hbar} \tilde{\mathbf{T}}(\vec{p}_t) \tilde{\psi}_t(\vec{p}_t), \quad (48)$$

$$\dot{\vec{q}}_t = m^{-1} \cdot \langle \tilde{\mathbf{p}}(\vec{p}_t) \rangle \tilde{\psi}_t(\vec{p}_t), \quad (49)$$

$$\dot{\vec{p}}_t = 0, \quad (50)$$

where  $[\tilde{\mathbf{T}}(\vec{p}_t)]_{KK'} = \delta_{KK'} T(\vec{p}^K(\vec{p}_t))$ . The exact solution of Eqs. (48)–(50) for any time  $t$  is

$$\tilde{\psi}_t(\vec{p}_t) = \tilde{\mathbf{U}}_T(t, \vec{p}_0) \tilde{\psi}_0(\vec{p}_0), \quad (51)$$

$$\vec{q}_t = \vec{q}_0 + tm^{-1} \cdot \vec{p}_0, \quad (52)$$

$$\vec{p}_t = \vec{p}_0. \quad (53)$$

Note that Eqs. (47) and (52), which appear to be first-order approximations, are exact since  $\partial \mathbf{V} / \partial \vec{q}(\vec{q}_t)$  commutes with  $\mathbf{U}_V(t, \vec{q}_t)$ , and  $\tilde{\mathbf{p}}(\vec{p}_t)$  with  $\tilde{\mathbf{U}}_T(t, \vec{p}_t)$ ; therefore,  $\langle \partial \mathbf{V} / \partial \vec{q}(\vec{q}_t) \rangle_{\tilde{\psi}_t(\vec{p}_t)}$  in Eq. (44) and  $\langle \tilde{\mathbf{p}}(\vec{p}_t) \rangle_{\tilde{\psi}_t(\vec{p}_t)}$  in Eq. (49) are time-independent.

The resulting, overall evolution operators (which also include the grid evolution) for the potential and kinetic splitting steps are

$$\mathbf{U}_{V,\text{adpt}}(\Delta t; \psi_0, \vec{q}_0) := \mathbf{U}_V(\Delta t, \vec{q}_0), \quad (54)$$

$$\begin{aligned} \mathbf{U}_{T,\text{adpt}}(\Delta t; \psi_0, \vec{q}_0, \vec{p}_0) \\ := \tilde{\mathbf{f}}(\vec{q}_{\Delta t}, \vec{p}_0) \tilde{\mathbf{U}}_T(\Delta t, \vec{p}_0) \mathbf{f}(\vec{q}_0, \vec{p}_0), \end{aligned} \quad (55)$$

respectively, where we have used that  $\vec{p}_0 = \vec{p}_{\Delta t}$  in Eq. (55) [which follows from Eq. (53)]. Evolution operators  $\mathbf{U}_{V,\text{adpt}}(\Delta t; \psi_0, \vec{q}_0)$  and  $\mathbf{U}_{T,\text{adpt}}(\Delta t; \psi_0, \vec{q}_0, \vec{p}_0)$  preserve the norm, which follows from Eq. (20) and from the fact that  $\mathbf{U}_V(\Delta t, \vec{q}_0)^\dagger \mathbf{U}_V(\Delta t, \vec{q}_0) = \tilde{\mathbf{U}}_T(\Delta t, \vec{p}_0)^\dagger \tilde{\mathbf{U}}_T(\Delta t, \vec{p}_0) = 1$ . A composition of norm-preserving operators is norm-preserving<sup>45</sup> and, therefore, any split-operator algorithm composed from  $\mathbf{U}_{V,\text{adpt}}(\Delta t; \psi_0, \vec{q}_0)$  and  $\mathbf{U}_{T,\text{adpt}}(\Delta t; \psi_0, \vec{q}_0, \vec{p}_0)$  is norm-preserving.

Time reversibility of  $\mathbf{U}_{V,\text{adpt}}(\Delta t; \psi_0, \vec{q}_0)$  follows because  $\mathbf{U}_V(-\Delta t, \vec{q}_0) \mathbf{U}_V(\Delta t, \vec{q}_0) = 1$ . Similarly,  $\mathbf{U}_{T,\text{adpt}}(\Delta t; \psi_0, \vec{q}_0, \vec{p}_0)$  is time-reversible because

$$\begin{aligned} \mathbf{U}_{T,\text{adpt}}(-\Delta t; \psi_{\Delta t}, \vec{q}_{\Delta t}, \vec{p}_0) \mathbf{U}_{T,\text{adpt}}(\Delta t; \psi_0, \vec{q}_0, \vec{p}_0) \\ = \tilde{\mathbf{f}}(\vec{q}_0, \vec{p}_0) \tilde{\mathbf{U}}_T(-\Delta t, \vec{p}_0) \mathbf{f}(\vec{q}_{\Delta t}, \vec{p}_0) \\ \times \tilde{\mathbf{f}}(\vec{q}_{\Delta t}, \vec{p}_0) \tilde{\mathbf{U}}_T(\Delta t, \vec{p}_0) \mathbf{f}(\vec{q}_0, \vec{p}_0) = 1, \end{aligned} \quad (56)$$

where we used Eq. (20) and the identity  $\mathbf{U}_T(-\Delta t, \vec{p}_0) \mathbf{U}_T(\Delta t, \vec{p}_0) = 1$ . A symmetric composition of time-reversible operators is time-reversible.<sup>45</sup> Therefore, all symmetric split-operator algorithms of form (6) that are composed from  $\mathbf{U}_{V,\text{adpt}}(\Delta t; \psi_0, \vec{q}_0)$  and  $\mathbf{U}_{T,\text{adpt}}(\Delta t; \psi_0, \vec{q}_0, \vec{p}_0)$  are time-reversible.

## H. Stability of the time-reversible adaptive grid

Equations (46), (47), (52), and (53) for the evolution of the grid centers are essentially the equations of the Verlet algorithm.<sup>42,46,47</sup> The stability<sup>42,48</sup> of the method from Sec. II G, therefore, depends mostly on the stability of the Verlet algorithm because the split-operator algorithms, by themselves, are stable for all  $\Delta t$ .

The Verlet algorithm applied to the harmonic oscillator is stable for time steps that satisfy

$$\Delta t < T_{\text{osc}} / \pi, \quad (57)$$

where  $T_{\text{osc}}$  is the oscillation period.<sup>42</sup> In higher-dimensional harmonic models, the restriction (57) on the time step must hold for the period  $T_{\text{osc}}$  of the fastest normal mode.<sup>42</sup>

## III. NUMERICAL EXAMPLES

### A. Three-dimensional harmonic model

To analyze the geometric and convergence properties of the algorithm proposed in Sec. II G, we devised a two-surface three-dimensional harmonic model of electronic excitation of a molecule. The initial vibrational state, determined using the ground-state potential energy surface, was propagated solely on the excited-state surface, following an impulsive electronic excitation. More precisely, the initial state for the propagation was the ground vibrational eigenstate,

$$\psi(\vec{q}) = (\pi \hbar)^{-D/4} \exp(-\vec{q}^2 / 2\hbar), \quad (58)$$

of the ground-state Hamiltonian,

$$\hat{H}_g = \sum_{l=1}^D \frac{\omega_l}{2} [(\hat{p}_l)^2 + (\hat{q}_l)^2], \quad (59)$$

where  $q_l$  is the  $l$ th ground-state normal mode coordinate,  $p_l$  is its conjugate momentum, and  $\omega_l$  is the associated vibrational frequency. After the electronic excitation,  $\psi(\vec{q})$  was propagated with the excited-state Hamiltonian

$$\hat{H}_e = \sum_{l=1}^D \frac{\omega_l}{2} \hat{p}_l^2 + \frac{1}{2} (\hat{q} - \vec{q}_0)^T \cdot K \cdot (\hat{q} - \vec{q}_0), \quad (60)$$

where  $\vec{q}_0$  is the displacement of the excited-state potential energy surface and  $K$  is a symmetric positive definite matrix;  $K$  is not diagonal because the excited-state normal modes were chosen to be Duschinsky rotated<sup>49</sup> with respect to the ground-state normal modes. For the dynamics, natural units (n.u.) were used:  $\hbar = \omega_2 = m_{\text{H}} = 1$ , where  $m_{\text{H}}$  is the mass of a hydrogen atom. The diagonal ( $K_{ll}$ ) and off-diagonal ( $K_{lm}$ ) elements of the  $K$  matrix, displacement  $\vec{q}_0$ , and ground-state vibrational frequency  $\omega_l$  in Eq. (60) are listed in Table I, which also contains

TABLE I. Parameters for the quantum dynamics of the harmonic model from Sec. III A. The parameters of the Hamiltonian (60) (the force constant  $K$ , displacement  $\vec{q}_0$ , and ground-state vibrational frequencies  $\vec{\omega}$ ), initial parameters of the adaptive grid ( $\vec{N}$ ,  $\vec{q}_{\text{ctr}}$ ,  $\Delta\vec{q}$ ), and the total propagation time are shown in natural units (n.u.) defined in Sec. III A.

Parameters	Values	Parameters	Values
$K_{11}$	1.997	$\omega_1$	2
$K_{22}$	1.015	$\omega_2$	1
$K_{33}$	2.48	$\omega_3$	2.5
$K_{12}$	-0.04	$N_1 = N_2 = N_3$	32
$K_{13}$	-0.017	$q_{\text{ctr},1} = q_{\text{ctr},2} = q_{\text{ctr},3}$	0
$K_{23}$	0.04	$\Delta q_1 = \Delta q_2 = \Delta q_3$	0.4375
$q_{0,1}$	-7	$t_f$	50
$q_{0,2} = q_{0,3}$	7		

the initial parameters of the adaptive grid and the total propagation time  $t_f$ .

To verify that grid adaptation does not decrease the accuracy of the solution, we compared the wavefunction  $\psi_t^{(\Delta t)}$  propagated using the adaptive grid with the time step  $\Delta t$  to the corresponding “benchmark” wavefunction  $\Psi_t^{(\Delta t)}$  propagated using a fixed grid. Indeed, the errors  $\|\psi_t^{(\Delta t)} - \Psi_t^{(\Delta t)}\|$  were minuscule (the errors were  $5 \times 10^{-11}$  at  $t = 0$ , and  $2 \times 10^{-10}$  at  $t = t_f$ ). The wavefunctions were propagated with the optimally composed tenth-order TVT split-operator algorithm with  $\Delta t = t_f/2^9$ . (See Ref. 45 and the references therein for a detailed discussion of composition schemes.) We used a high-order integrator with a small time step so that the error was dominated by grid adaptation, and not by time discretization. Both  $\vec{q}^-$  and  $\vec{p}^-$  ranges of the fixed grid were chosen to be twice larger than the ranges of the adaptive grid because the amplitude of the adaptive grid’s oscillation was approximately equal to its range. In order that the fixed and adaptive grids had the same density, the fixed grid was chosen to have  $128 \times 128 \times 128$  points.

Figure 1(a) shows that the expectation value of position is computed correctly with the adaptive grid, even when the wavefunction moves beyond the range of the initial grid. In fact, Fig. 1(b) shows that the error of the position expectation value is minuscule (of the order of  $10^{-11}$ ) for all times; the slow linear increase in the error is due to the accumulation of roundoff errors.

Figure 2 demonstrates that the compositions<sup>11,33–36</sup> of the proposed algorithm from Sec. II G achieve the predicted higher orders of accuracy. The figure also demonstrates the divergence of the discretization errors  $\|\psi_{t_f}^{(\Delta t)} - \psi_{t_f}^{(\Delta t/2)}\|$  when the composition substep size,  $|\gamma_k|\Delta t$ , does not satisfy condition (57). Note that the accumulation of roundoff errors does not allow the discretization errors to reach below  $\approx 10^{-10}$ .

Higher-order methods allow the use of much larger time steps without sacrificing accuracy (see Fig. 2). However, the efficiency can only be inferred from the depen-

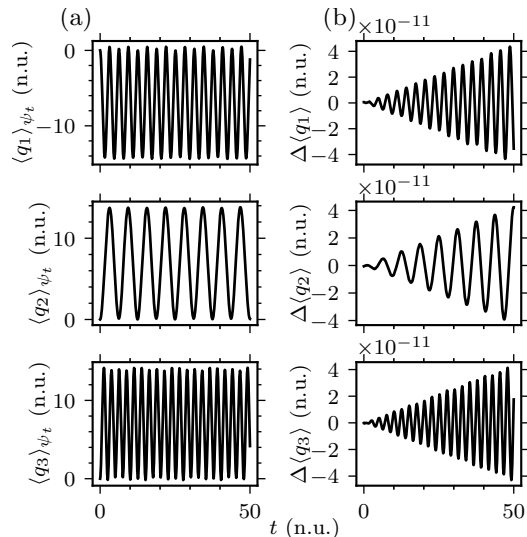


FIG. 1. Accuracy of the adaptive grid used for quantum dynamics of the three-dimensional harmonic model (60) from Sec. III A. (a) Position expectation values  $\langle q_i \rangle_{\psi_t}$  computed on the adaptive grid. (b) Difference  $\Delta \langle q_i \rangle := \langle q_i \rangle_{\psi_t} - \langle q_i \rangle_{\Psi_t}$  between the position expectation values computed on the adaptive grid ( $32 \times 32 \times 32$  points) and fixed grid ( $128 \times 128 \times 128$  points).

dence of the discretization error on the computational cost, which we measure by the central processing unit (CPU) time. Figure 3 shows that a tenfold speedup is already achieved by using the optimal tenth-order instead of the second-order algorithm to reach a moderate discretization error of  $10^{-2}$ . A much greater (10000-fold) speedup is possible if a small error ( $< 10^{-10}$ ) is desired.

Because a split-operator propagation is equivalent to an exact propagation with an effective, time-dependent Hamiltonian, the energy  $E_t^{(\Delta t)} = \langle \psi_t^{(\Delta t)} | \hat{H} | \psi_t^{(\Delta t)} \rangle$  is conserved only approximately. Figure 4(a) shows that the energy is conserved to the same order of accuracy [ $\mathcal{O}(\Delta t^m)$ ] as the wavefunction. Figures 4(b) and (d) demonstrate that the compositions of the proposed algorithm are exactly norm-preserving and time-reversible as already justified analytically in Sec. II G. In Sec. II E, we showed that the grid adaptation leads to the non-conservation of the inner product. Figure 4(c) may, therefore, be misleading because the inner product appears to be conserved. However, this is not true in general, as shown later on the example of collinear He–H<sub>2</sub> scattering (see Sec. III B).

In all panels of Fig. 4 the slow increase in the error for decreasing time steps is because of the accumulation of roundoff errors; therefore, the (minuscule) errors are larger for methods with more composition steps per time step.<sup>11</sup> Panels (b), (c), and (d) show that, on the other hand, the errors diverge for large time steps  $\Delta t$  because of the instability of the Verlet algorithm (see Sec. II H); larger errors result from methods with a larger maximum composition coefficient [ $\max_k |\gamma_k|$ , see Eq. (57)].

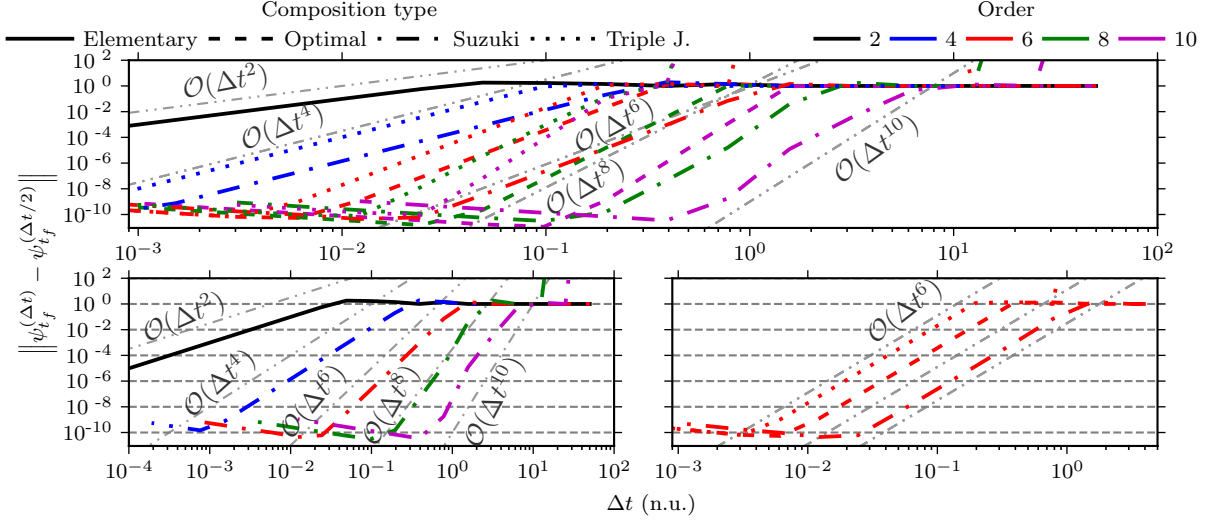


FIG. 2. Convergence (up to the tenth-order) of the wavefunction as a function of the time step in the harmonic system from Sec. III A. In this figure and Figs. 3–5, we only show the results for the compositions of the TVT algorithm. Gray straight lines indicate predicted orders of convergence. Top: all discussed methods; bottom left: methods composed through Suzuki’s fractal<sup>33</sup>; bottom right: sixth-order methods.

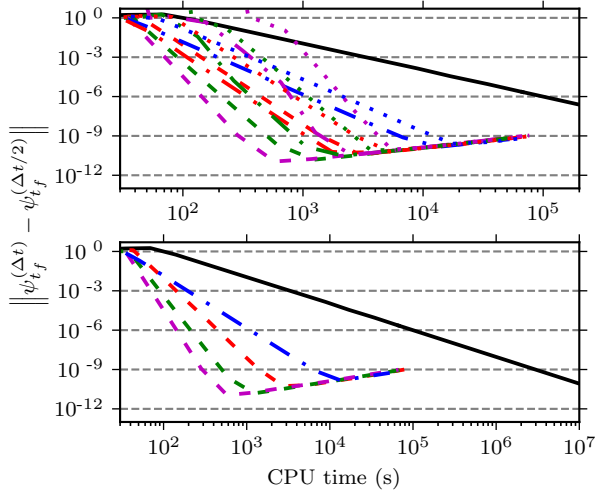


FIG. 3. Efficiency of the compositions of the proposed algorithm (see Sec. II G) in the harmonic system from Sec. III A. Results of the second-order TVT algorithm were extrapolated using the line of best fit beyond CPU time =  $7 \times 10^4$  s to highlight the higher efficiency of the higher-order methods. Top: all discussed methods; bottom: optimally composed methods (Suzuki’s fractal is the optimal fourth-order composition scheme<sup>35,36,45</sup>). Line labels are the same as in Fig. 2.

Figure 5 confirms that the naïve adaptive grid approach is not time-reversible while the algorithm proposed in Sec. II G is. Note that for very small time steps ( $\Delta t \leq 10^{-2}$ ), the solution is essentially exact, and even the naïve adaptive grid approach becomes effectively time-reversible. The bottom panel of Fig. 5 shows, however, that for a fixed time step  $\Delta t$ , the time propagation

on the naïve adaptive grid is not time-reversible already after a short propagation time  $t$ ; the breaking of time reversibility is an inherent property of the naïve adaptive grid.

## B. Collinear He–H<sub>2</sub> scattering

As a more challenging test, we also applied the algorithm proposed in Sec. II G to a very anharmonic system. Following Ref. 29, we simulated the collinear He–H<sub>2</sub> scattering using a modified<sup>39</sup> Secret–Johnson<sup>38</sup> potential energy surface,

$$V_{\text{SJ}}(\vec{q}) = D(1 - e^{-\beta q_1})^2 + e^{-\alpha(q_2 - q_1)}, \quad (61)$$

where  $\beta = 0.158$  n.u.,  $D = 20$  n.u., and  $\alpha = 0.3$  n.u. The natural units (n.u.) are different from those defined in Sec. III A:  $\hbar = 1$  as before, but  $\sqrt{2D\beta^2/m_1} = m_1 = 1$  instead. In Eq. (61),  $q_1$  is the vibrational coordinate of H<sub>2</sub>, and  $q_2$  is the distance between the He atom and the center of mass of H<sub>2</sub>.<sup>38</sup> In this coordinate system,  $m_1 = 1$  n.u. and  $m_2 = 2/3$  n.u.<sup>29,38</sup> The Hamiltonian for this problem is  $\hat{H}_{\text{scat}} = T(\hat{p}) + V_{\text{SJ}}(\hat{q})$ , where  $T(\hat{p})$  has the form (3).

Identically to Ref. 29, the initial state is a product of two one-dimensional Gaussian wavepackets

$$\begin{aligned} \psi_{(1)}(q) &= (\pi\hbar)^{-1/4} \exp(-q^2/2\hbar), \\ \psi_{(2)}(q) &= (\pi\sigma_0^2)^{-1/4} \exp[-(q - q_0)^2/2\sigma_0^2 + ip_0(q - q_0)/\hbar]. \end{aligned} \quad (62)$$

The Gaussian wavepacket  $\psi_{(2)}(q)$  is sufficiently narrow and far from the interaction region so that there is no

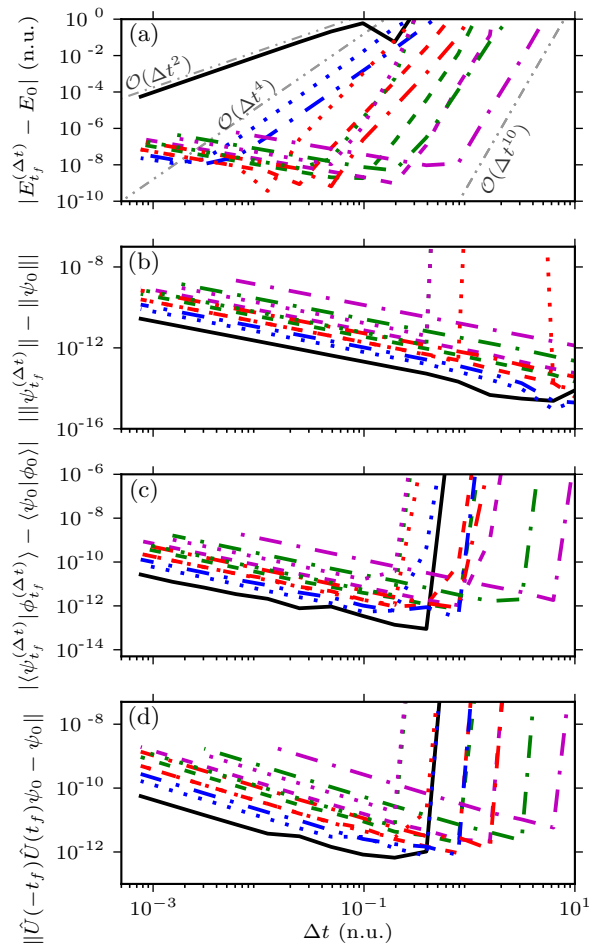


FIG. 4. Conservation of geometric properties by the compositions of the proposed algorithm from Sec. II G as a function of the time step in the harmonic system from Sec. III A: (a) energy [ $E_0 = 140.389$  n.u.], (b) norm, (c) inner product, and (d) time reversibility.  $\phi_0$  is wavepacket (58) displaced by  $q_1 = -1$  n.u. and  $q_2 = q_3 = 1$  n.u. (hence,  $\langle \psi_0 | \phi_0 \rangle = 0.472$ ). Time reversibility is measured by the distance between  $\psi_0$  and the forward-backward propagated state, i.e.,  $\psi_0$  propagated forward in time for  $t_f$  and then backward in time for  $t_f$ . Gray straight lines indicate predicted orders of convergence  $\mathcal{O}(\Delta t^m)$  for  $m = 2, 4$ , and  $10$ . Line labels are the same as in Fig. 2.

significant initial interaction between He and  $\text{H}_2$  ( $\sigma_0^2 = 8$  n.u. and  $q_0 = 24$  n.u.). A negative initial momentum ( $p_0 = -3.56$  n.u.) ensures a collision at a later time.

Figure 6 shows the error of the wavefunction propagated using either the adaptive or fixed grid, both with the same number of grid points. The error of the wavefunction propagated using the adaptive grid remains reasonably small ( $< 10^{-3}$ ) for six times longer than the error of the corresponding wavefunction on the fixed grid. The significance is that for a given number of grid points, determined, e.g., by the available memory, the time scale of a simulation can be extended by grid adaptation.

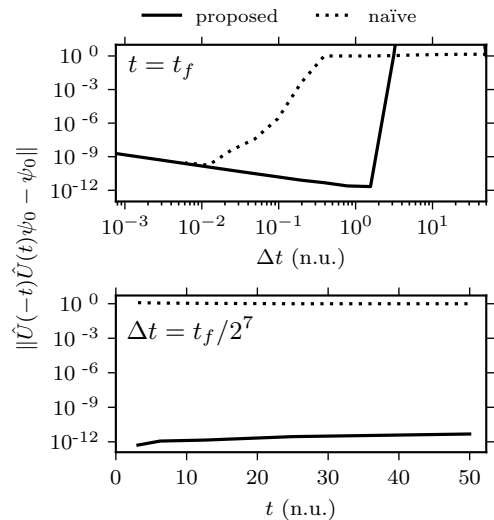


FIG. 5. Time reversibility of the naïve (see Sec. II F) and proposed (see Sec. II G) split-operator algorithms on adaptive grids in the harmonic system from Sec. III A. Both split-operator algorithms were composed to the tenth order using the optimal scheme. Top: time reversibility as a function of the time step  $\Delta t$  for a fixed total propagation time  $t$ . Bottom: time reversibility as a function of the total propagation time  $t$  for a fixed time step  $\Delta t$ .

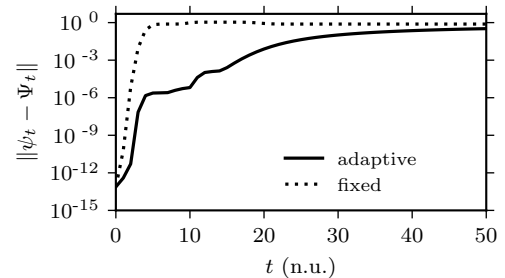


FIG. 6. Error  $\|\psi_t - \Psi_t\|$  of the wavefunction  $\psi_t$  propagated on either the adaptive or fixed grid (both with  $128 \times 128$  points) in the He- $\text{H}_2$  scattering from Sec. III B.  $\Psi_t$  is the “exact” reference wavefunction propagated on a fixed grid with  $128 \times 2048$  points. The initial  $q_1$  range of all grids was  $(-14$  n.u.,  $14$  n.u.). The initial  $q_2$  range was  $(0$  n.u.,  $48$  n.u.) for both grids with  $128 \times 128$  points and  $(-50$  n.u.,  $400$  n.u.) for the reference fixed grid. This and all following figures were produced using the optimal tenth-order composition of the VTV algorithm with  $\Delta t = 0.1$  n.u.

Figure 7 displays the time dependence of the expectation value of  $\bar{q}$  and of its error. Panel (a) shows that the collision between He and  $\text{H}_2$  induces the vibration of  $\text{H}_2$ , which was originally in its ground vibrational state. Panel (b) shows that the error of the position expectation value was reasonably small until  $t \approx 20$  n.u. on the adaptive grid.

Finally, in Fig. 8, we show that the proposed algorithm preserves the geometric invariants even in the collinear



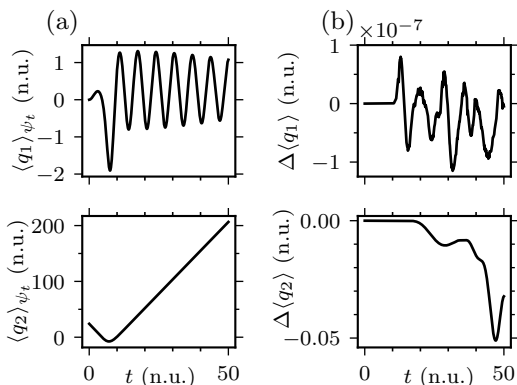


FIG. 7. Accuracy of the adaptive grid for simulating the He–H<sub>2</sub> scattering (see Sec. III B) (a) Expectation values of position computed on the adaptive grid. (b) The difference between the position expectation values computed on the adaptive grid ( $128 \times 128$  points) and reference fixed grid ( $128 \times 2048$  points).

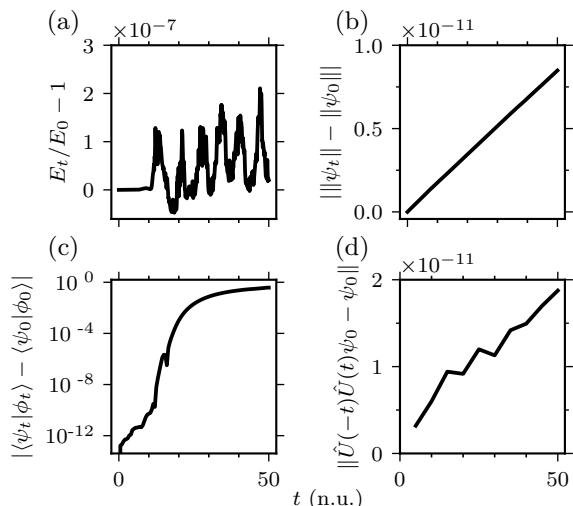


FIG. 8. Geometric properties of the algorithm proposed in Sec. II G applied to the He–H<sub>2</sub> scattering from Sec. III B: (a) energy, (b) norm, (c) inner product, (d) time reversibility. The time reversibility is defined in the same way as in the caption of Fig. 4.  $\phi_0$  is a Gaussian wavepacket identical to  $\psi_0$ , the two-dimensional initial Gaussian wavepacket from Sec. III B, except that  $p_0$  in Eq. (62) is  $-3.0$  n.u. instead of  $-3.56$  n.u. (hence,  $|\langle \psi_0 | \phi_0 \rangle| = 0.534$ ).

scattering of He–H<sub>2</sub>, where the wavepacket is more delocalized than in the harmonic example from Sec. III A. As expected, the norm [Fig. 8(b)] and time reversibility [Fig. 8(d)] are preserved exactly (the slow linear increase of the invariants is again due to the accumulation of roundoff errors). On the other hand, the energy [Fig. 8(a)] and inner product [Fig. 8(c)] are not conserved. In particular, the apparent conservation of the inner product observed in Sec. III A is indeed not general.

## IV. CONCLUSION

We have described a split-operator algorithm combined with an adaptive phase-space grid whose center moves according to the wavepacket’s expectation values of position and momentum. By propagating the grid center exactly and simultaneously with the wavefunction, the symmetry and time reversibility were built into the proposed algorithm. Adapting the grid reduces the number of required grid points while maintaining high accuracy in situations where the wavepacket remains localized. Examples include harmonic systems or short-time dynamics in moderately anharmonic systems. On the example of He–H<sub>2</sub> scattering, we showed that the proposed algorithm is also suitable for longer-time dynamics if only a moderate accuracy of the wavepacket is required, i.e., when one can ignore small parts of the wavepacket escaping through the boundaries of the adaptive grid.

We showed both analytically and numerically that the time reversibility is lost by the naïve grid adaptation. Then, we introduced an amendment that recovered the time reversibility. The geometric properties of the resulting algorithm, namely norm preservation, conditional stability, symmetry, and time reversibility, were demonstrated analytically as well as numerically on two different model systems.

Because of its symmetry, the proposed algorithm can be composed to obtain higher-order integrators. We verified that these higher-order integrators are more efficient compared to the second-order integrator if high accuracy is desired. As an additional benefit, the proposed algorithm requires no adjustable parameters for the grid adaptation because the grid center follows the exact trajectory of the wavepacket’s expectation values of position and momentum.

Finally, we hope that the proposed time-reversible integrator for the time-dependent Schrödinger equation on an adaptive grid could serve as a benchmark for more approximate methods, such as the thawed Gaussian approximation,<sup>50–52</sup> that rely on the wavepacket remaining localized for relevant time scales.

The authors acknowledge the financial support from the European Research Council (ERC) under the European Union’s Horizon 2020 research and innovation programme (grant agreement No. 683069 – MOLEQULE) and thank Tomislav Begušić for useful discussions.

<sup>1</sup>E. J. Heller, *The semiclassical way to dynamics and spectroscopy* (Princeton University Press, Princeton, NJ, 2018).

<sup>2</sup>V. Engel, H. Metiu, R. Almeida, R. Marcus, and A. H. Zewail, *Chem. Phys. Lett.* **152**, 1 (1988).

<sup>3</sup>R. Kosloff, *J. Phys. Chem.* **92**, 2087 (1988).

<sup>4</sup>G. Stock, C. Woywod, W. Domcke, T. Swinney, and B. S. Hudson, *J. Chem. Phys.* **103**, 6851 (1995).

<sup>5</sup>T. Begušić, A. Patoz, M. Šulc, and J. Vaníček, *Chem. Phys.* **515**, 152 (2018).

<sup>6</sup>M. Ben-Nun, J. Quenneville, and T. J. Martínez, *J. Phys. Chem. A* **104**, 5161 (2000).

<sup>7</sup>M. P. Bircher, E. Liberatore, N. J. Browning, S. Brickel, C. Hofmann, A. Patoz, O. T. Unke, T. Zimmermann, M. Chergui,

- P. Hamm, U. Keller, M. Meuwly, H. J. Woerner, J. Vaníček, and U. Rothlisberger, *Struct. Dyn.* **4**, 061510 (2017).
- <sup>8</sup>M. D. Feit, J. A. Fleck, Jr., and A. Steiger, *J. Comp. Phys.* **47**, 412 (1982).
- <sup>9</sup>D. J. Tannor, *Introduction to Quantum Mechanics: A Time-Dependent Perspective* (University Science Books, Sausalito, 2007).
- <sup>10</sup>C. Lubich, *From Quantum to Classical Molecular Dynamics: Reduced Models and Numerical Analysis*, 12th ed. (European Mathematical Society, 2008).
- <sup>11</sup>E. Hairer, C. Lubich, and G. Wanner, *Geometric Numerical Integration: Structure-Preserving Algorithms for Ordinary Differential Equations* (Springer Berlin Heidelberg New York, 2006).
- <sup>12</sup>J. Roulet, S. Choi, and J. Vaníček, *J. Chem. Phys.* **150**, 204113 (2019).
- <sup>13</sup>D. Kosloff and R. Kosloff, *J. Comp. Phys.* **52**, 35 (1983).
- <sup>14</sup>H.-D. Meyer, U. Manthe, and L. S. Cederbaum, *Chem. Phys. Lett.* **165**, 73 (1990).
- <sup>15</sup>U. Manthe, H. Meyer, and L. S. Cederbaum, *J. Chem. Phys.* **97**, 3199 (1992).
- <sup>16</sup>G. A. Worth, H.-D. Meyer, H. Köppel, L. S. Cederbaum, and I. Burghardt, *Int. Rev. Phys. Chem.* **27**, 569 (2008).
- <sup>17</sup>H. Wang and M. Thoss, *J. Chem. Phys.* **119**, 1289 (2003).
- <sup>18</sup>G. Avila and T. Carrington Jr, *J. Chem. Phys.* **131**, 174103 (2009).
- <sup>19</sup>V. Gradinaru, *SIAM J. Num. Analysis* **46**, 103 (2008).
- <sup>20</sup>D. Lauvergnat and A. Nauts, *Spectrochim. Acta A* **119**, 18 (2014).
- <sup>21</sup>S. A. Smolyak, *Dokl. Akad. Nauk SSSR* **148**, 1042 (1963).
- <sup>22</sup>J. F. Thompson, Z. U. Warsi, and C. W. Mastin, *Numerical grid generation: foundations and applications*, Vol. 45 (North-holland Amsterdam, 1997) Chap. 11.
- <sup>23</sup>C. L. Lobreore and R. E. Wyatt, *Phys. Rev. Lett.* **82**, 5190 (1999).
- <sup>24</sup>R. E. Wyatt, *J. Chem. Phys.* **111**, 4406 (1999).
- <sup>25</sup>R. E. Wyatt and E. R. Bittner, *J. Chem. Phys.* **113**, 8898 (2000).
- <sup>26</sup>R. E. Wyatt, *J. Chem. Phys.* **117**, 9569 (2002).
- <sup>27</sup>K. H. Hughes and R. E. Wyatt, *Chem. Phys. Lett.* **366**, 336 (2002).
- <sup>28</sup>H. Lu and A. D. Bandrauk, *J. Chem. Phys.* **115**, 1670 (2001).
- <sup>29</sup>E. Sim and N. Makri, *J. Chem. Phys.* **102**, 5616 (1995).
- <sup>30</sup>S. Adhikari and G. D. Billing, *J. Chem. Phys.* **113**, 1409 (2000).
- <sup>31</sup>B. Barkakaty and S. Adhikari, *J. Chem. Phys.* **118**, 5302 (2003).
- <sup>32</sup>J. Lill, G. Parker, and J. Light, *Chem. Phys. Lett.* **89**, 483 (1982).
- <sup>33</sup>M. Suzuki, *Phys. Lett. A* **146**, 319 (1990).
- <sup>34</sup>H. Yoshida, *Phys. Lett. A* **150**, 262 (1990).
- <sup>35</sup>W. Kahan and R.-C. Li, *Math. Comput.* **66**, 1089 (1997).
- <sup>36</sup>M. Sofroniou and G. Spaletta, *Optim. Method Softw.* **20**, 597 (2005).
- <sup>37</sup>P. Ehrenfest, *Z. Phys* **45**, 455 (1927).
- <sup>38</sup>D. Secrest and B. R. Johnson, *J. Chem. Phys.* **45**, 4556 (1966).
- <sup>39</sup>J. Campos-Martínez and R. D. Coalson, *J. Chem. Phys.* **93**, 4740 (1990).
- <sup>40</sup>H. F. Trotter, *Proc. Amer. Math. Soc.* **10**, 545 (1959).
- <sup>41</sup>G. Strang, *SIAM J. Numer. Anal.* **5**, 506 (1968).
- <sup>42</sup>B. Leimkuhler and S. Reich, *Simulating Hamiltonian Dynamics* (Cambridge University Press, 2004).
- <sup>43</sup>M. Frigo and S. G. Johnson, *Proc. IEEE* **93**, 216 (2005).
- <sup>44</sup>P. R. Halmos, *Finite dimensional vector spaces* (Princeton University Press, 1942).
- <sup>45</sup>S. Choi and J. Vaníček, *J. Chem. Phys.* **150**, 204112 (2019).
- <sup>46</sup>L. Verlet, *Phys. Rev.* **159**, 98 (1967).
- <sup>47</sup>D. Frenkel and B. Smit, *Understanding molecular simulation*, 2nd ed. (Academic Press, 2002).
- <sup>48</sup>N. P. Bhatia and G. P. Szegő, *Dynamical systems: stability theory and applications*, Vol. 35 (Springer, 2006).
- <sup>49</sup>F. Duschinsky, *Acta Physicochim. U.R.S.S.* **7**, 551 (1937).
- <sup>50</sup>E. J. Heller, *J. Chem. Phys.* **62**, 1544 (1975).
- <sup>51</sup>M. Wehrle, M. Šulc, and J. Vaníček, *J. Chem. Phys.* **140**, 244114 (2014).
- <sup>52</sup>T. Begušić, M. Cordova, and J. Vaníček, *J. Chem. Phys.* **150**, 154117 (2019).